Multi-scale modelling of moisture diffusion coupled with stress distribution in CFRP laminated composites

Published in Composite Structures 138(2016) 295-304.

Multi-scale modelling of moisture diffusion coupled with stress distribution in CFRP laminated composites

M. Meng, M. J. Rizvi, H.R. Le*, S. M. Grove

School of Marine Science and Engineering, Plymouth University, United Kingdom

*Corresponding author: huirong20@yahoo.co.uk, Fax: +44 (0)1752 586101

Abstract

Laminated composite structures operating in a marine environment are subject to moisture ingress. Due to the slow diffusion process of moisture, the distribution of moisture is not uniform so that the laminates can develop hygrothermal stresses. An accurate prediction of the moisture concentration and the associated hygrothermal stress is vital to the understanding of the effect of marine environment on failure initiation. The present paper investigates the time-dependent moisture diffusion and the stress distribution in carbon fibre reinforced polymeric (CFRP) composites by means of experimental study and Finite Element Analysis (FEA). Samples were made from CFRP pre-preg autoclave-cured, and then immersed in fresh water and sea water at a constant 50°C for accelerated moisture diffusion. Laminates with $[0]_{16}$, $[90]_{16}$, $[\pm45]_{4s}$ lay-up sequences were investigated. A multiscale 3D FEA model was developed to evaluate the interfacial stresses between polymer matrix and carbon fibre and the stress distribution in the composite laminates. The analysis revealed that both the stress distribution and stress level are time-dependent due to moisture diffusion, and the interphase between fibres and matrix plays an important role in both the process of moisture diffusion and the stress/strain transfer. The interlaminar shear stresses of the laminates induced by hygrothermal expansion exhibited a significant specimen edge effect. This is correlated with the experimental observations of the flexural failure of laminates.

Keywords: Laminated composite, Moisture diffusion, Multi-scale modelling, FEA

An earlier version of this paper was presented at ICCS18, Lisbon, Portugal, 15-18 June 2015.

Published in Composite Structures 138(2016) 295-304.

1. Introduction

Fibre reinforced plastic (FRP) composites were first used in marine structures at the end of World War II when the US Navy was seeking to reduce the maintenance and production costs of ship hulls[1]. In contrast to the aerospace industry, where a high strength to weight ratio is essential, the use of marine composites was prompted by their superior environmental resistance and fatigue life. FRP composites have been used for critical marine structures, such as propellers [2], hulls [3], shafts [4], pipes and tanks [5]. The US shipment of marine composites in 2014 was about $0.3 billion and this value is expected to grow by 65% by 2020 [6]. The growth of marine composites is partly due to the development of marine renewable energy and other offshore applications. Since FRP composites can be tailored into complex shapes, these materials are used, for example, to construct tidal turbine blades[7].

The challenges for composite materials to be used in the marine environment include the long exposure time to moisture and temperature, as well as microorganisms and numerous ionic species present in seawater. Recently, Summerscales[8] gave a general review on the marine environmental effects on the durability of FRP composites. The loss in the mechanical properties of composite materials is mainly attributed to the plasticisation of polymeric matrix. However, the previous investigations of the moisture effects of current commercial FRP composites in the marine environment are based on the accelerated laboratory studies and mainly considered moisture diffusion effects on the polymeric matrix.

The hygrothermal degradation of FRP composites can be divided into two categories: the reduction of the glass transition temperature T_g [9], and the stresses induced by hygrothermal expansion [10]. Specifically, moisture absorption reduces the T_g of the polymer matrix due to plasticisation resulting from the interruption of van der Waals bonds between the polymer chains [11], which also leads to the decrease of matrix-dominated stiffness and strength of FRP composites. Usually, the effects of moisture and temperature are considered simultaneously to determine the synergistic effects of these two exposures. According to previous studies, temperature does not change the saturated moisture content but accelerates the process of diffusion. This relation between temperature and moisture diffusivity is commonly known as Arrhenius equation[12], which introduced the terms of activation energy. Shen and Springer [13] pointed out that, for many polymer composites, the temperature distribution approaches equilibrium about one million times faster than the moisture concentration. Therefore, the short time-scale fluctuations of temperature can be neglected with regard to the evolution of moisture content.

An earlier version of this paper was presented at ICCS18, Lisbon, Portugal, 15-18 June 2015.

Moisture diffusion in isotropic materials, such as a pure polymer, is governed by Fick's first and second laws [14]. However, many previous publications, e.g. [13, 15-17], have shown that moisture diffusion in polymer-based composites can also be described by Fick's laws. For a thin plate ($w/h >> 1, l/h >> 1$), the moisture content (M) can be derived from Fick's first and second laws as[18]:

$$M = M_\infty \left[1 - \exp\left(-7.3 \left(\frac{Dt}{h^2} \right)^{0.75} \right) \right] \quad (1)$$

where M_∞ is the saturated moisture concentration, D is the apparent moisture diffusivity, t is the time, w, l, h are the width, length and thickness respectively.

The apparent diffusivity can be calculated from the measurements at the early stages of diffusion (where M is proportional to the square root of time):

$$D = \pi \left(\frac{h}{4M_\infty} \right)^2 \left(\frac{M_2 - M_1}{\sqrt{t_2} - \sqrt{t_1}} \right)^2 \quad (2)$$

In a sample of finite dimensions, the longitudinal (D_L) and transverse (D_T) diffusivities can be used to compensate for the diffusion from the sample's edges[19]:

$$\sqrt{D} = \frac{w+h}{w} \sqrt{D_T} + \frac{h}{l} \sqrt{D_L} \quad (3)$$

The apparent diffusivity D is determined by equation (2), while D_L and D_T can be determined by samples with different dimensions using equation (3).

Previous experimental observations [13, 20] have demonstrated that, for polymeric composites, the expansion induced by moisture absorption is generally a linear function of moisture content if the range of moisture content is less than 2%. Since the moisture distribution inside composites is non-uniform throughout any given ply, classical laminate theory (CLT) is unlikely to predict the hygrothermal expansion and the associated stresses for a laminate with a complex lay-up[21]. The effects of induced hygrothermal stress, along with additional external mechanical loading, on the physical properties of CFRP appear not to have been investigated extensively.

The aim of the present work is to investigate the moisture diffusion at both micro- and macro-scales and the coupling effects between hygrothermal expansion and bending, by means of experimental and numerical approaches. This work mainly focuses on the effects of moisture

An earlier version of this paper was presented at ICCS18, Lisbon, Portugal, 15-18 June 2015.

diffusion on the transverse properties of composite, particularly the role of the interphase between fibre and matrix. A two-dimensional FEA model was developed to simulate the moisture diffusion and stress/strain transfer at micro-scale (i.e. the ply), while a three-dimensional FEA model was developed to simulate the moisture diffusion, hygrothermal expansion and the coupling of hygrothermal stress with bending at macro-scale (i.e. the laminate).

2. Experiment setup

2.1 Material preparation

High strength UD carbon fibre/epoxy pre-preg (Cytec 977-2-12kHTS) was used in this study. The pre-preg was hand laid on a flat mould tool, then vacuum-bagged and autoclave cured at 180^{o}C and 85psi (0.6 MPa) pressure, according to the manufacturer's instructions[22]. The calculated fibre volume fraction was $V_f = 58\%$. Three typical lay-up sequences were chosen for the composite laminates: $[0]_{16}$, $[90]_{16}$, $[+45/-45]_{4s}$. These three lay-ups are the simplest examples of laminates which show a range of different laminate stacking: the unidirectional laminates (longitudinal $[0]_{16}$, transverse $[90]_{16}$) are fibre and matrix dominated respectively to show the strongest and weakest mechanical properties, while the angle-ply ($[\pm45]_{4s}$) laminate presents intermediate properties. The study of these three common lay-ups could provide a general view of the effects of fibre orientation on moisture diffusion and hygrothermal stresses.

The laminates were to be tested in bending following the ISO standards[23, 24] which required a nominal plate thickness of 2 mm. Therefore all of the laminates in the present work were made up of 16 plies to satisfy the ISO standards.

The matrix is a high temperature (180°C) curing toughened epoxy resin with 212°C glass transition temperature which is formulated for autoclave moulding. The aromatic epoxide-amine network[25] consists of bisphenol A diglycidyl ether (commonly abbreviated BADGE, or DGEBA) and diaminodiphenyl sulfone (DDS). The PAN-based carbon fibres present parallel graphite layers to the surface near the skin region [26]. Therefore, the transverse elastic properties of carbon fibre are significantly lower than the longitudinal properties. Studies have suggested that the transverse modulus is about 10% of its longitudinal value [27-29].

An earlier version of this paper was presented at ICCS18, Lisbon, Portugal, 15-18 June 2015.

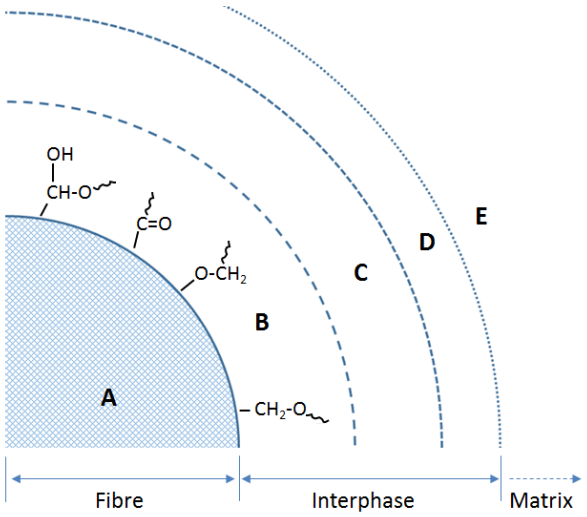

Fig.1 Five-region model of fibre-epoxy interface

In terms of fibre composite, the interface is usually considered as the chemically bonded junction between resin (including the size) and the fibre surface. The link between resin and fibre is very complicated. Kardos [30] suggested that the link contains five zones as shown in Fig.1, where A is the fibre, B is a layer of reactive site on the fibre surface, C is the third-phase interlayer referred to above, D is the size, and E is the matrix. The typical thickness of the interphase is 0.1μm on 7μm diameter fibres, which varies for different types of fibre surface treatment[31]. According to Waltersson's observation [32], approximate 33% of the region of the fibre/matrix interface was not well bonded therefore it was suggested that the mechanical properties of the interphase (e.g. elastic modulus and tensile strength) could be estimated by 1/3 lower than the matrix.

An optical image of the microstructure is required to build the corresponding FEA geometry. The specimens were set in a mould and encapsulated by transparent resin, and then ground and polished to be optically flat using a polishing media containing 1.5μm diamond particles, as shown in Fig.2.

Fig.2 Polished UD ($[0]_{16}$), UT ($[90]_{16}$) and AP ($[\pm45]_{4s}$) specimens for the microscopic study

An earlier version of this paper was presented at ICCS18, Lisbon, Portugal, 15-18 June 2015.

2.2 Fibre packing analysis

Regardless of the stacking sequence of a composite laminate, all the fibres in each ply are assumed to be aligned parallel to each other within a single ply. There are several fibre packing assumptions to predict the fibre volume fraction, such as hexagonal and square lattices[3],

$$V_f = \frac{\pi}{2\sqrt{3}}\left(\frac{r}{R}\right)^2 \quad \text{(Hexagonal)} \qquad (4\text{-}1)$$

$$V_f = \frac{\pi}{4}\left(\frac{r}{R}\right)^2 \quad \text{(Square)} \qquad (4\text{-}2)$$

where V_f is the fibre volume fraction, r is the radius of a single fibre and R is half of the central distance between two adjacent fibres.

Theoretically, it is predicted that the maximum fibre volume fraction is $V_f = 0.907$ for hexagonal lattice and 0.785for a square lattice by equation (4). For many carbon fibres, the average radius is approximately 3.5μm. Considering the inversion of equation (4), the central distance between two adjacent fibres within a composite ply with $V_f = 0.58$ can be calculated as 8.751μm (hexagonal) and 8.144μm (square).

Due to the inevitable limitations of the current manufacturing technique, the fibre lattice cannot be perfectly hexagon or square. Fig.3 shows the real fibre lattice of a unidirectional laminate (Cytec 977-2-12kHTS). A mixture of the hexagonal and square lattices can be seen from the figure, with quite a few resin rich volumes.

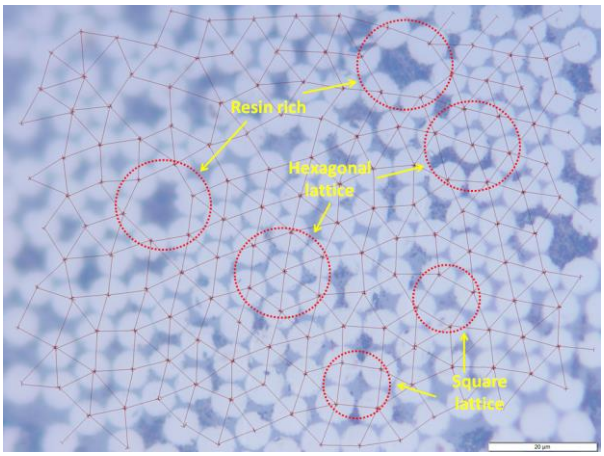

Fig.3 Fibre lattice of a unidirectional laminate

Fig.4 shows the statistics of the central distance between two adjacent fibres of Cytec 977-2-12kHTS unidirectional laminate ($V_f = 0.58$) based on the fibre lattice shown in Fig.3. The microscopic images were taken from an optical microscope using 1000 times magnification (OLYMPUS BX60M), and the fibre distances were measured by OLYMPUS STREAM

An earlier version of this paper was presented at ICCS18, Lisbon, Portugal, 15-18 June 2015.

software (version 1.9). The measurements of the fibre distances were then imported into MATLAB for curve fitting using DFITTOOL toolbox. The best fit was three-parameter Weibull function given by[33]:

$$f(d) = \frac{k}{\lambda}\left(\frac{d-d_0}{\lambda}\right)^{k-1} e^{-\left(\frac{d-d_0}{\lambda}\right)^k} \qquad (5)$$

where λ is the scale factor, k is shape factor, d is the fibre spacing and d_0 is the threshold fibre spacing. For HTS-12K/977-2 unidirectional laminate $\lambda = 1.39 \pm 0.02, k = 1.50 \pm 0.023$ and $d_0 = 6.5\mu m$. A reasonably good fit was obtained.

It is interesting to note that the average central distance from the statistical analysis (7.705μm) is shorter than the predictions of either a square lattice (8.144μm) or a hexagonal lattice (8.751μm) based on equation (4). One possible reason is that the compaction of fibres tends to squeeze the resin out; resulting in resin rich volumes which reduce the overall fibre volume fraction.

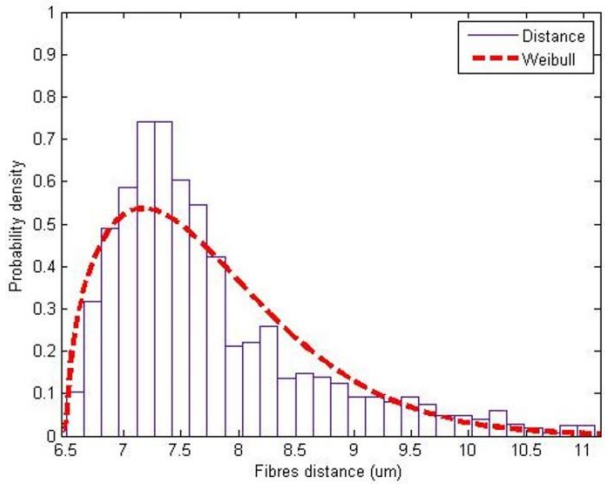

Fig.4 Statistics of fibre distance of a unidirectional laminate. Approximate two thousand specimens are included in the statistics.

The gaps between the adjacent fibres are very narrow, showing only 0.7μm on average. It can be seen from Fig.4 that some fibre separations are less than 7μm (the average diameter of carbon fibres). One possible reason is that the radius of these fibres is slightly smaller than the average value. Nevertheless, Fig.4 suggests that there are many fibres presenting a very narrow gap which affect both the moisture distribution and stress distribution.

2.3 Diffusion and bending tests

Fresh water (tap water) and sea water were used for the diffusion test to investigate the degradation of composite properties. The sea water used was collected from the English

Channel near Plymouth harbour, and the water was refreshed every month during the tests. The salinity of the sea water was varying with seasons and depth, and the values were in the range of 3.4%-3.5% in weight. The salinity was similar with values in the open literatures so that the chemical composition can be referred to ASTM D1141[34].

Before being immersed in the water, all of the specimens were oven-dried at 70°C for 48 hours. The specimens were constrained and separated by breathing nylon cloth before being immersed. In order to accelerate the diffusion process, all the samples were placed in an oven at a constant temperature of 50°C. Following the ASTM standard[18], the specimens were taken out at intervals to measure the moisture content and hygrothermal expansion. The moisture content by weight was measured by a weight scale with 0.01 mg accuracy, while the dimensions were measured by a vernier calliper with 0.01 mm nominal accuracy. At least five specimens of each lay-up were immersed in each chamber, and the mean values were calculated. Equations (2) and (3) were used to calculate the apparent moisture diffusivity, with longitudinal (D_L) and transverse (D_T) moisture diffusivities obtained from the UD ($[0]_{16}$) and UT ($[90]_{16}$) data (UT: Unidirectional Transverse).

The measurements showed a very rapid weight gain during the first week of immersion and saturation of the composite after three months at a weight gain of 0.9% with a transverse moisture diffusivity $D_T = 2\times10^{-13} m^2/s$ and longitudinal moisture diffusivity $D_L = 3.6\times10^{-13} m^2/s$. Substituting the densities of fibre ($1.78\times10^3 kg/m^3$), matrix ($1.31\times10^3 kg/m^3$) and the value of fibre volume fraction (58%), the saturation and moisture diffusivity of matrix can be calculated as 2.7% and $6\times10^{-13} m^2/s$ respectively at the test temperature. It is interesting to note that the difference in moisture diffusivity between fresh water and sea water was negligible.

Bending tests (following the ISO standard[24]) were carried out to investigate the elastic properties both in dry and saturated conditions. At least five samples in each group were tested, and the properties transverse to fibres were focused on in the presented work due to their sensitivity to moisture diffusion. The flexural strength and modulus of the dry UT specimens were 117±5 MPa and 8.4±0.3 GPa respectively, while the same properties in the saturated condition were 102±4 MPa and 9.0±0.2 GPa respectively.

3. FEA modelling

Two scales of FEA model were built to study the moisture diffusion within CFRP composite laminates and its coupling with external mechanical loading. At the micro scale, a 2D model was constructed according to the real distribution of fibres within one single ply to investigate the moisture diffusion behaviour. At the macro scale, a 3D model was developed based on

the actual laminate lay-up to investigate the impact of moisture diffusion and external load on the interlaminar shear stresses.

3.1 Micro model

The geometry of the micro scale model was taken directly from the optical microscope image to capture the real distribution of fibres within a single ply, but assuming that the fibres were perfectly circular, as shown in Fig. 5. The FEA model contained two components: (a) species transport was used to simulate the moisture diffusion within the matrix and interphase, therefore the surface ply (ply 16) was extracted for the FEA geometry; (b) structural mechanics was employed to calculate the stress/strain transfer among the three phases, as well as the coupling between hygrothermal expansion and external loading.

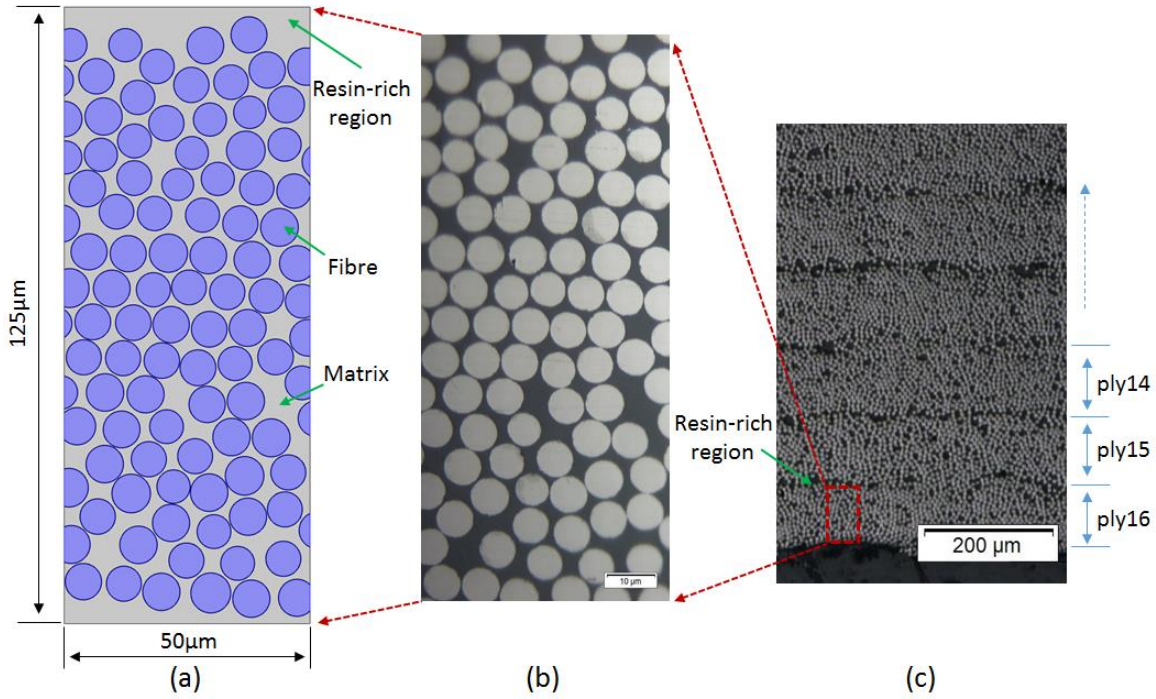

Fig.5 Optical microscopic image of a UT specimen and schematics of FEA model

It can be seen from Fig.5 (c) that there was a resin-rich volume between two adjacent layers; therefore it is reasonable to extract a single ply for the modelling by applying the continuous boundary condition. For the species transport component, the lower surface was defined as being at the saturated moisture concentration given by:

$$c_{\max} = \frac{\rho_m M_\infty^m}{18\times 10^{-3}} \qquad (6)$$

where ρ_m is the density of matrix, and 18×10^{-3} kg/mol is the molar mass of water. Substituting the matrix saturation (2.7%) into equation (6), the boundary moisture concentration can be calculated as $1965\,mol/m^3$.

It can also be seen from Fig.5 (a) that the fibres are very close to each other so that the stress concentration due to the barrier layer effect could be induced during moisture diffusion. It is well known that the moisture diffusivity of the interphase should be different from that of the matrix. Therefore, a sensitivity study of the interphase diffusivity was carried out to investigate this barrier effect.

Due to the bending moment applied to the laminate, the bottom surface of the laminate was under maximum tension, and the tensile stress at the 15th and 16th plies near the bottom was calculated to be 102 MPa and 117 MPa respectively. For the structural mechanics component, a distributed tensile stress was applied on the left side of the model while the right side was defined as symmetric plane. Fig.6 shows the schematics of the boundary conditions for both species transport component and structural mechanics component.

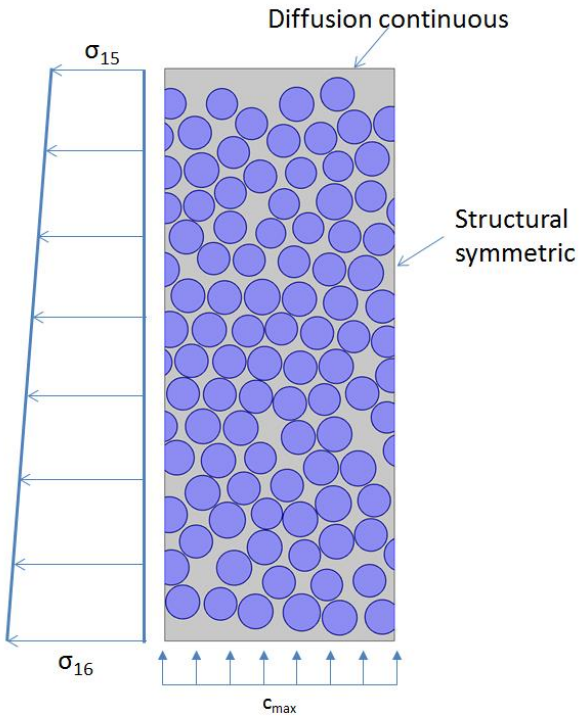

Fig.6 The boundary conditions for the multiphysics micro model: species transport and structural mechanics

The mechanical properties of the fibre and matrix were obtained from the product technical datasheet[22], and the diffusion properties of the matrix was taken as the measured value in section 2.3. Table 1 gives the material properties used for the micro-model. The properties of the interphase shown in Table 1 were for the baseline case, and these values were used for the parametric study.

An earlier version of this paper was presented at ICCS18, Lisbon, Portugal, 15-18 June 2015.

An area with dimensions of $125\mu m \times 50\mu m$ was considered with 125 μm being the thickness of each ply. There were three phases in the model including fibres, interphase and matrix. The diameter of the fibres varied with an average value of 7μm[35], while the thickness of the interphase was 0.1μm as the baseline case, which is equivalent to approximately 4% of the weight of fibres. The calculated fibre volume fraction was 58% which was the same as the experimental value.

Table 1 Mechanical and chemical properties of carbon fibre and epoxy

	E_1 (GPa)	$E_2 = E_3$ (GPa)	$\nu_{12} = \nu_{13}$	ν_{23}	D $(10^{-13} m^2/s)$	M_∞
Fibre	238	24	0.2	0.4	-	-
Matrix	3.5	3.5	0.34	0.34	6.0	2.7%
Interphase	2.6	2.6	0.34	0.34	6.0	2.7%

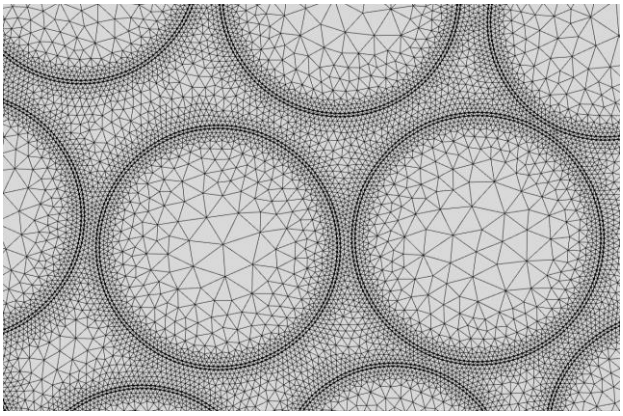

Fig.7 A local view of the mesh, showing the three phases in the micro model

The model was solved using COMSOL Multiphysics [36]. The automatic meshing method of COMSOL was employed to generate the mesh. Approximately 250k triangular elements were created. Fig.7 shows a magnified view of the mesh which shows detailed meshes of the three phases within the composite. The interphase and the adjacent regions were refined to capture the stress concentration effect and the fibres barrier effect.

3.2 Macro-model

As described in section 3.1, the micro model was a 2D plane strain approximation of a unidirectional composite specimen. The hygrothermal effect was not taken into account in the micro model because only free expansion was induced within the resin region under a simply supported boundary condition. However, for a laminate with a complicated stacking sequence, stress/strain can be induced by the hygrothermal expansion between the adjacent plies, and such induced strain/stress can be coupled with the external loading. In the present study, the

interlaminar shear stress of angle-ply laminate was emphasized because it plays an important role in the initiation of fracture of laminate in bending.

The macro-model was inherited from the authors' previous 3D FEA study of CFRP laminates[37] by adding the species transport component, and the coupling term (hygrothermal strain) was introduced to link the species transport and structural mechanics components:

$$\varepsilon^{CHE} = \frac{18\times10^{-3} c\beta}{\rho_c} \tag{7}$$

where ρ_c is the density of composite and β is coefficient of hygrothermal expansion (CHE) which can be calculated by the 'rule of mixtures' [10]:

$$\begin{cases} \beta_1 = \dfrac{E_m}{E_1}\dfrac{\rho_c}{\rho_m}\beta_m \\ \beta_2 = (1+\nu_m)\dfrac{\rho_c}{\rho_m}\beta_m - \beta_1\nu_{12} \end{cases} \tag{8-1}$$

Where

$$\rho_c = \rho_f V_f + \rho_m(1-V_f) \tag{8-2}$$

For the species transport component, all surfaces were fixed at a constant concentration which was calculated from equation (6) to be $800\,mol/m^3$. For the structural mechanics component, the boundary conditions corresponded to three-point bending, and the external loading was the same as the maximum value recorded in the bending tests (for the angle-ply laminate, $F_{\max} = 1395N$). Table 2 shows the material properties and the loading of species transport/structural mechanics components.

Table 2 Material properties of lamina and the loading for macro model ($[\pm45]_{4s}$)

Longitudinal modulus E_1	139 GPa
Transverse modulus $E_2 = E_3$	8.8 GPa
In-plane shear modulus $G_{12} = G_{13}$	4.7 GPa
Transverse shear modulus G_{23}	3.0 GPa
In-plane Poisson's ratio $\nu_{12} = \nu_{13}$	0.26
Transverse Poisson's ratio ν_{23}	0.48
Longitudinal diffusivity D_1	$3.6\times10^{-13} m^2/s$
Transverse diffusivity $D_2 = D_3$	$2.2\times10^{-13} m^2/s$
Longitudinal CHE β_1	0

An earlier version of this paper was presented at ICCS18, Lisbon, Portugal, 15-18 June 2015.

Transverse CHE $\beta_2 = \beta_3$	0.49

4. Results and discussion

4.1 Moisture diffusion

As discussed in section 3.1, the barrier layer effect develops due to the narrow gap between fibres. The diffusion rate extracted from the micro model was significantly lower than that observed in the experiment if the diffusivity of the interphase (D_{in}) was assumed to be the same as for the matrix in the FEA model. A parametric study was carried out to investigate the sensitivity of the interphase diffusivity. Fig.8 shows the comparison of the fit of the measurement to Fick's law and the predictions by the micro model for three levels of D_{in} : the same, five times, or ten times that of the matrix. The results suggested that the FEA prediction matched the experiment well when the D_{in} value was ten times that for the matrix. This is in agreement with the previous reports that the diffusivity of the interphase is much higher than that of the matrix.

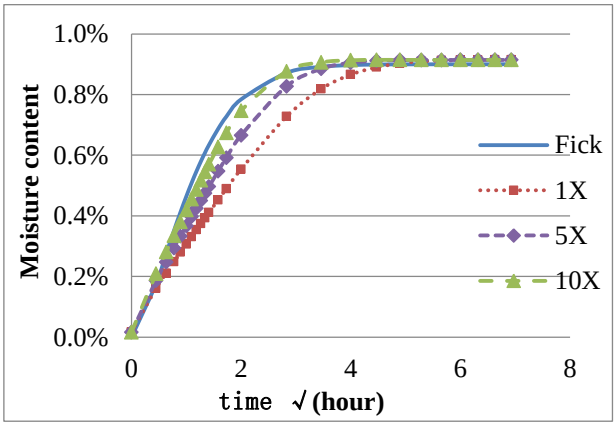

Fig.8 Comparison of mass gain: Fick's fit and FEA computation with various values of D_{in} .

A previous study of the carbon fibres/epoxides reaction [32] has shown that the mechanical modulus of the interphase is a fraction lower than the matrix, which may lead to a higher capability to attract water molecules. This is one of the possible reasons that the moisture diffusivity of the interphase presents a higher value.

According to equation (1), the time to saturation is exponential to the thickness of the specimen. The moisture can penetrate one ply thickness with relatively low concentration within a short time of immersion. Indeed, the moisture concentration reached saturation after 24 hours in the micro-model, compared to 90 days for the whole (16 ply) experimental laminate. Fig.9 shows the moisture distribution after one hour of immersion (D_{in} was 10 times that of the matrix). A magnified view of the interphase shows a smooth moisture

distribution which indicates the moisture distribution was not affected by the difference of diffusivities of the two phases of resin (the bulk and interphase).

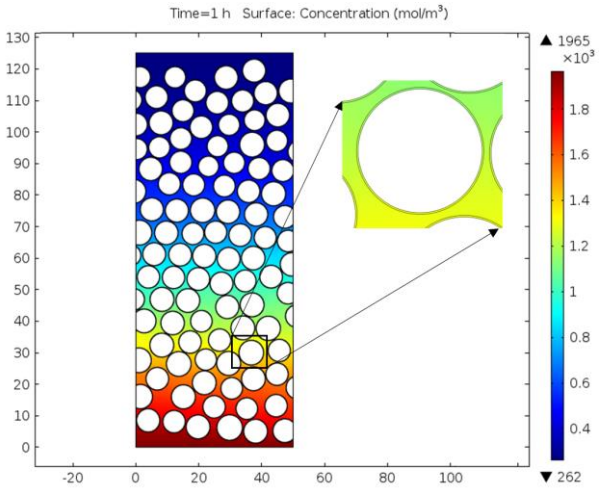

Fig.9 Moisture distribution in the micro model after one hour immersion (dimension unit: μm)

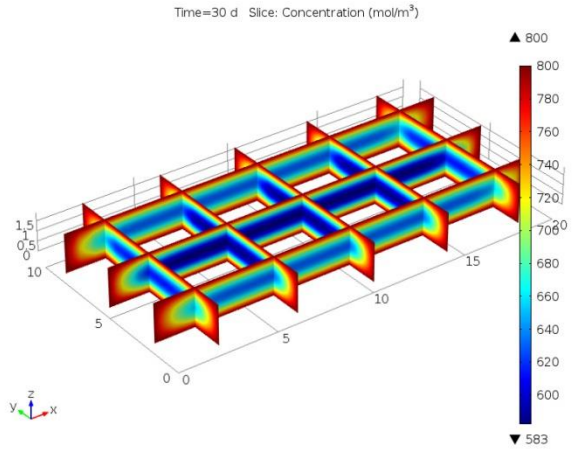

Fig.10 Moisture distribution of macro-model at specific slice sections for angle-ply laminate after one month immersion (dimension unit: mm)

Although the longitudinal diffusivity is 60% higher than the transverse, as shown in Table 2, the time-dependent moisture concentration in all three laminates ($[0]_{16}$, $[90]_{16}$, $[\pm45]_{4s}$) were quite similar. Fig.10 shows the FEA results of the macro model for moisture distribution within the angle-ply laminate in slice-view after one month of water immersion indicating different depth of water penetration in longitudinal and transverse directions. However, the slice plot shows a smooth distribution of moisture concentration regardless of the ply orientations.

4.2 Stress distribution

The mechanism of stress transfer among the three phases can be evaluated from the micro FEA model. The influence of the elastic modulus of the interphase was captured through a parametric study. Because of the random distribution of fibres, the first principal stress and

strain along an arbitrarily chosen line through-thickness were extracted. Fig.11 and Fig.12 show the first principal stress and strain distributions respectively along a line at x=25μm for the cases of $E_{in} = E_m$ and $E_{in} = 0.75E_m$.

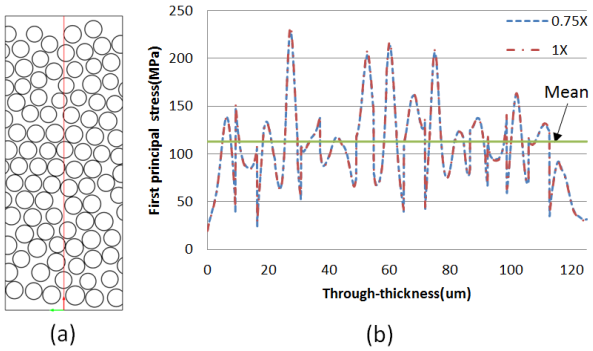

Fig.11 (a) Schematics of stress distribution and the chosen line for the stress plot; (b) First principal stress distribution along the chosen line. The mean value is also shown in the figure.

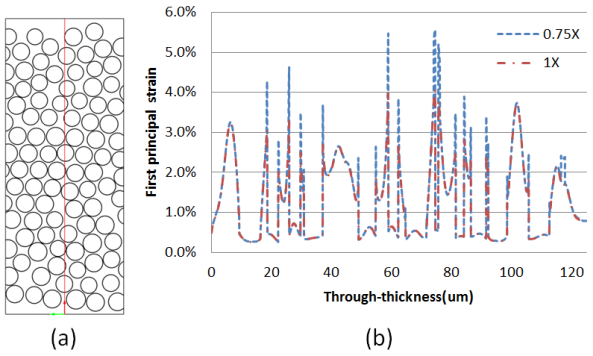

Fig.12 (a) Schematics of the chosen line for the strain plot; (b) First principal strain distribution along the chosen line.

Significant stress concentration can be seen in Fig.11 (b), and the peaks correspond to the fibre barrier regions located near the fibre surface. Eventual fracture may initiate at these regions with the combination of fibre surface peeling, fibre/interphase delamination, and matrix fracture. These peak stresses have exceeded the tensile strength of the matrix (81 MPa) and some of them even exceeded its flexural strength (197 MPa), according to the values given in the manufacturer's datasheet. The average value matched the applied load on the boundary (110MPa). The sensitivity study of the interphase modulus showed that the two curves almost overlapped each other, which means that a lower value of E_{in} did not change the stress distribution among the three phases.

The strain distribution in Fig.12 (b) gives more typical plot for the interaction among the three phases. The relative flat valleys show the strain in the fibres. Many extremely sharp peaks are evident at points where the chosen line crossed the fibre barrier regions. According to the previous studies, the ultimate failure strain of epoxy falls into the range of 5%-7% [10], which is close to the peak strains extracted from the micro model. Fig.13 is a local view of

An earlier version of this paper was presented at ICCS18, Lisbon, Portugal, 15-18 June 2015.

the strain distribution indicating that the stress concentration occurs at the narrow gaps between adjacent fibres.

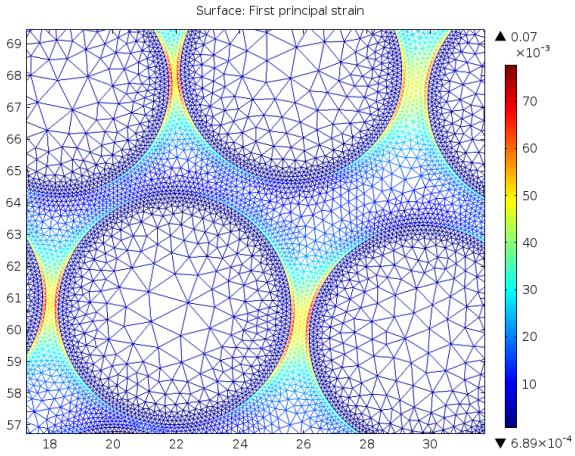

Fig.13 Distribution of the first principal strain. Peak values were found at interphases.

Fig.11 and Fig.12 illustrate the variation of mechanical behaviours of the first principal stress/strain in the sensitive study of the elastic modulus of interphase. Since the first principal stress is independent of the value of E_{in}, stress distributions along five chosen paths near the central were extracted to study the stress concentration in case of $E_{in} = E_m$, shown in Fig.14. Compared with Fig.9 (x=25μm), Fig.14 shows extremely high values of the stress concentration on each path at the fibre barrier region, indicating the possibility of micro crack initiation.

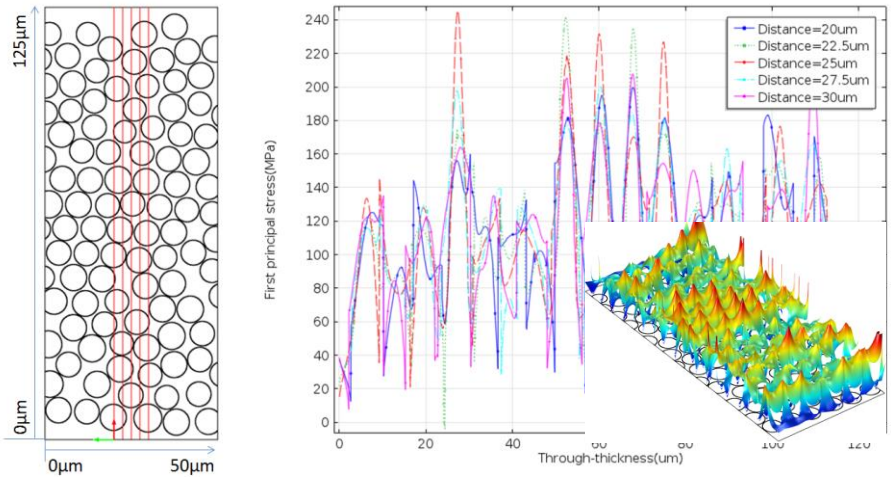

Fig.14 The distributions of the first principal stress along five chosen paths in the central

Fig.15 shows the distributions of interlaminar shear stress obtained from the macro FEA model along three chosen through-thickness lines in the angle-ply laminate. A significant edge effect can be seen in Fig.15 (a) and (b), however the extremely high value of interlaminar shear stress decayed significantly inside the laminate within a distance of two ply thicknesses. It can also be seen that the coupling of hygrothermal expansion had changed

the distribution of interlaminar shear stress so that the stress was asymmetric about the mid-plane, as shown in Fig.15 (b). The positions of peaks shifted to the tensile side. The maximum value of interlaminar shear stress showed an increase of about 15% after water absorption, compared with the dry condition.

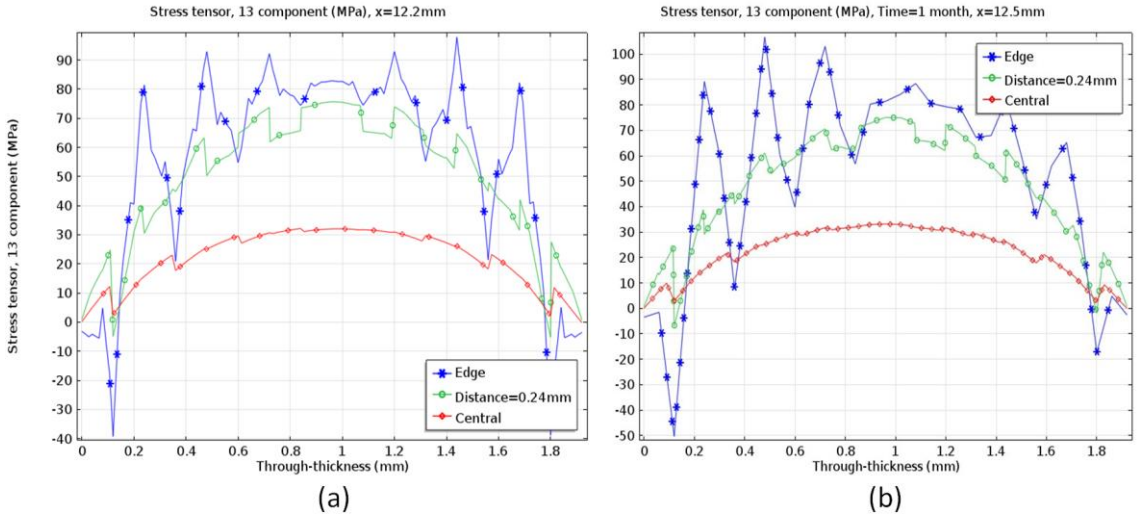

Fig.15 Through-thickness distribution of interlaminar shear stress of macro model for angle-ply laminate: (a) dry condition and (b) after one-month immersion.

4.3 SEM examination

Scanning eletronic microscopy (SEM) images were taken to compare with the FEA results by examining the interface of fibre/epoxy at the fracture surface, in order to investigate the failure mechanism. The fracture debris was taken from the UT laminate, including tests in the dry condition or after water immersion. The samples were coated with gold/palladium before being examined in SEM. Fig.16 shows the particular fracture surfaces under the two conditions.

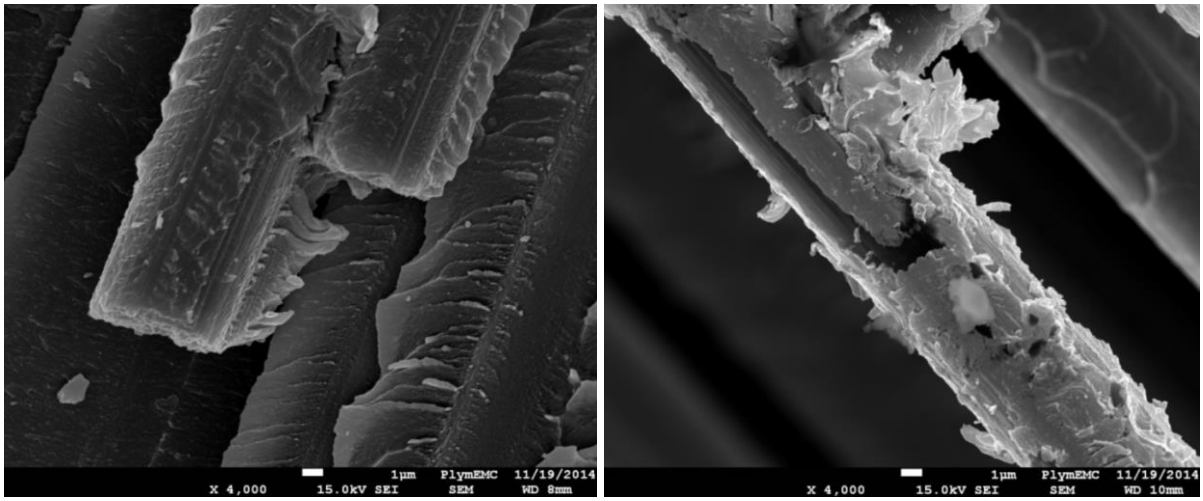

(a) **(b)**

Fig.16 SEM images of fracture surface: (a) dry condition, and (b) saturation

An earlier version of this paper was presented at ICCS18, Lisbon, Portugal, 15-18 June 2015.

In dry condition, the epoxy was still attached to the carbon fibre, so that the fractured polymer showed a brittle wave-like morphology which is similar with Bescom and Gweon's[38] and Greenhalgh's studies[39], as shown in Fig.16 (a). Without water ingression, the epoxy provided adequate adhesion to the carbon fibre, and the failure mode presented as the combination of epoxy tensile fracture and debonding of fibre/epoxy interphase. After moisture ingress, the carbon fibres showed sections of bare surface which indicates that the adhesion of interphase/epoxy on carbon fibre had deteriorated and debonded, as shown in Fig.16 (b). It is also noted that the matrix breaks in a more ductile manner. These observations confirm that the moisture ingress leads to plasticisation of the resin and the weakening of the fibre/resin interface.

5. Conclusions

The failure mechanisms of composite material are very complicated, particularly when considering the additional effects of water immersion. A realistic 2D FEA model has been developed to analyse the moisture diffusion and stress/strain transfer at the micro scale while a 3D FEA model has analysed the hygrothermal effect coupled with bending. The experimental results showed a good agreement with the FEA solutions.

This study suggests that the moisture diffusivity of the interphase must be about one order of magnitude higher than that of the matrix, in order to reproduce the fibre barrier effect. Due to the very slow diffusion process, the moisture concentration within both micro/macro models exhibited a smooth distribution despite the significant difference in diffusivities of interphase/matrix and ply orientations.

The micro model revealed a significant stress concentration at the fibre barrier regions. A lower interphase modulus had no effect on the stress distribution, but increased the strain at the fibre barrier regions which made the failure mode more complicated. The coupling effect of hygrothermal expansion induced a significant interlaminar shear stress edge effect at the interfaces of adjacent plies, and the study showed a decrease by about 15% in interlaminar shear strength when the CFRP composite is moisture-saturated. The SEM analysis has shown a variety of matrix fracture morphologies and the effects of degradation of the fibre/matrix interface on the failure mechanisms of CFRP composites in a marine environment.

The model predictions described in this paper have helped to understand the failure mechanisms of CFRP composites in the marine environment. The multi-scale modelling

approach developed can be applied to a selection of samples of microstructure to extract the statistical properties of moisture diffusion and mechanical properties of composite laminates.

6. Acknowledgments

The authors would like to thank Professor Long-yuan Li for his advice on FEA modelling, Dr Richard Cullen for his kind help with composites manufacturing, Terry Richards for his support of the mechanical tests, Dr John Summerscales for his kind comments, and the financial support of the School of Marine Science and Engineering, Plymouth University.

7. References

1. Greene E. Use of Fiber Reinforced Plastics in the Marine Industry; 1990.
2. Marsh G. A new start for marine propellers? Reinforced Plastics 2004;48(11):34-38.
3. Hull D, Clyne T. An introduction to composite materials: Cambridge university press; 1996.
4. Greene E. Marine composites: Eric Greene Associates; 1999.
5. Selvaraju S, Ilaiyavel S. Applications of composites in marine industry. J. Eng. Res. Stud., II 2011:89-91.
6. ACMA. www.acmanet.org. American Composites Manufacturers Association 2015.
7. Mohan M. The advantages of composite materials in marine renewable energy structures. RINA Marine Renewable Energy Conference 2008 2008.
8. Summerscales J. Durability of Composites in the Marine Environment. In: Davies P, Rajapakse YD, editors. Durability of Composites in a Marine Environment: Springer; 2014. p. 1-13.
9. Zafar A, Bertocco F, Schjødt-Thomsen J, Rauhe JC. Investigation of the long term effects of moisture on carbon fibre and epoxy matrix composites. Composites Science and Technology 2012;72(6):656-66.
10. Gibson RF. Principles of composite materials mechanics. McGraw-Hill 1994(ISBN O-07-023451-5).
11. Wolff EG. Moisture effects on polymer matrix composites. SAMPE Journal(USA) 1993;29(3):11-19.
12. Gibson RF. Principles of composite material mechanics: CRC press; 2011.
13. Shen C-H, Springer GS. Moisture absorption and desorption of composite materials. Journal of Composite Materials 1976;10(1):2-20.
14. Smith WF, Hashemi J. Foundations of materials science and engineering: Mcgraw-Hill Publishing; 2006.
15. Vinson JR. Advanced composite materials-environmental effects: ASTM International; 1978.
16. Cairns DS, Adams DF. Moisture and thermal expansion of composite materials. U,S. ARMY RESEARCH OFFICE Report 1981;UWME-DR-101-104-1.
17. Springer GS. Environmental effects on composite materials: Technomic Pennsylvania; 1981.
18. ASTM-D5229/5229M. Standard Test Method for Moisture Absorption Properties and Equilibrium Conditioning of Polymer Matrix Composite Materials. 2014.
19. Pomies F, Carlsson L, Gillespie J. Marine environmental effects on polymer matrix composites. ASTM SPECIAL TECHNICAL PUBLICATION 1995;1230:283-303.
20. Cairns D, Adams D. Moisture and thermal expansion properties of unidirectional composite materials and the epoxy matrix. Environmental Effects on Composite Materials 1984;2:300-16.
21. Meng M, Rizvi MJ, Grove SM, Le HR. Effects of hygrothermal stress on the failure of CFRP composites. Composite Structures 2015;133:1024-35.
22. Cytec. CYCOM 977-2 Epoxy resin system. www.cytec.com. Technical data sheet 2012.

An earlier version of this paper was presented at ICCS18, Lisbon, Portugal, 15-18 June 2015.

23. ISO14130. Fibre-reinforced plastic composites -- Determination of apparent interlaminar shear strength by short-beam method. 1997.
24. ISO14125. Fibre-reinforced plastic composites -- Determination of flexural properties. 1998.
25. Rasoldier N, Colin X, Verdu J, et al. Model systems for thermo-oxidised epoxy composite matrices. Composites Part A: Applied Science and Manufacturing 2008;39(9):1522-29.
26. Johnson D. Structure-property relationships in carbon fibres. Journal of Physics D: Applied Physics 1987;20(3):286.
27. Bowles DE, Tompkins SS. Prediction of coefficients of thermal expansion for unidirectional composites. Journal of Composite Materials 1989;23(4):370-88.
28. Voyiadjis GZ, Kattan PI. Mechanics of Composite Materials with MATLAB. 2005(Springer).
29. Hyer MW. Stress analysis of fiber-reinforced composite materials: DEStech Publications, Inc; 2009.
30. Kardos J. The role of the interface in polymer composites—some myths, mechanisms, and modifications. Molecular characterization of composite interfaces: Springer; 1985. p. 1-11.
31. Hughes JDH. The carbon fibre/epoxy interface—A review. Composites Science and Technology 1991;41(1):13-45.
32. Waltersson K. ESCA studies of carbon fibres: Part II—Surface reactions of carbon fibres with epoxides. Composites Science and Technology 1985;22(3):223-39.
33. MATWORKS. MATLAB reference manual. 2013.
34. ASTM-D1141. Standard Practice for the Preparation of Substitute Ocean Water: ASTM International West Conshohocken. 2008.
35. Toho-Tenax-HTS Technical data sheet. www.tohotenax-eu.com.
36. COMSOL. COMSOL Multiphysics reference manual. 2013.
37. Meng M, Le HR, Rizvi MJ, Grove SM. 3D FEA modelling of laminated composites in bending and their failure mechanisms. Composite Structures 2015;119:693-708.
38. Bascom WD, Gweon SY. Fractography and failure mechanisms of carbon fibre-reinforced composite materials. London & New York: Elsevier; 1990.
39. Greenhalgh E. Failure analysis and fractography of polymer composites: Elsevier; 2009.

An earlier version of this paper was presented at ICCS18, Lisbon, Portugal, 15-18 June 2015.